Sigg, http://www.jgp.org/cgi/content/full/jgp.201210859/DC1

Derivation of linkage equations for the generalized Scheme 3

The general gating scheme (Scheme 3) illustrated in Fig. 4 of the main text possesses a binary pore, but the other modality-specific domains may be composite, characterized by multiple equilibrium constants (***J***, ***K***) and internal allosteric factors (***F***, ***G***). The aim of this section is to derive linkage equations for Scheme 3, given by Eqs. 37a–d in the main text. Fig. S1 illustrates the sub-schemes corresponding to each linkage cycle. The linkage diagram of Scheme 3 parsed in the order $\mathrm{L}\rightarrow\mathbf{J}_{[\mathrm{G}]}\rightarrow\mathbf{K}_{[\mathrm{F}]}$ is given by:

$$\left(\mathbf{K}_{[\mathrm{F}]}\xrightarrow{\mathbf{J}_{[\mathrm{G}]}}\mathbf{K}_{[\mathrm{F}]}\mathbf{E}\right)^4\xrightarrow{L}\left(\mathbf{K}_{[\mathrm{F}]}\mathbf{C}\xrightarrow{\mathbf{J}_{[\mathrm{G}]}\mathbf{D}}\mathbf{K}_{[\mathrm{F}]}\mathbf{CE}\right)^4$$

(SCHEME 3)

To construct the partition function, we follow the same parsing scheme as in the diagram, beginning with the voltage-dependent particles L. The first-order parsing of the partition function is, as usual:

$$Z = Z_C{}^4 + LZ_O{}^4,$$

where Z_C and Z_O are closed- and open-channel CPFs. The closed-state CPF Z_C contains all equilibrium parameters except for L, ***C***, and ***D***, which only come into play when the channel opens. We can write $Z_C = f_1(\boldsymbol{J}, \boldsymbol{K}, \boldsymbol{E}, \boldsymbol{F}, \boldsymbol{G}, \boldsymbol{\chi})$, where f_1 is a polynomial function. An unspecified variable $\boldsymbol{\chi}$ is included to allow for the possibility of additional protomers (such as pH- or other ligand-sensing moieties). The open-state CPF Z_O is also a function of f_1, but with ***JC*** and ***KD*** substituting for ***J*** and ***K***, so that we may write $Z_O = f_1(\boldsymbol{JD}, \boldsymbol{KC}, \boldsymbol{E}, \boldsymbol{F}, \boldsymbol{G}, \boldsymbol{\chi}_L)$. Note the distinction between $\boldsymbol{\chi}$ and $\boldsymbol{\chi}_L$, which is important if $\boldsymbol{\chi}$ is coupled to the pore. Assuming f_1 is fairly insensitive to the differential influences of $\boldsymbol{\chi}$ and $\boldsymbol{\chi}_L$, the CPF ratio Z_O/Z_C can be written as (compare with Eq. 22 in the main text):

$$\frac{Z_O}{Z_C} = \frac{f_1(\boldsymbol{JD},\boldsymbol{KC},\boldsymbol{E},\boldsymbol{F},\boldsymbol{G},\boldsymbol{\chi}_L)}{f_1(\boldsymbol{J},\boldsymbol{K},\boldsymbol{E},\boldsymbol{F},\boldsymbol{G},\boldsymbol{\chi}_L)},$$

$$\left(\frac{Z_O}{Z_C}\right)_{\boldsymbol{J}(\pm)} = \langle \boldsymbol{C}\rangle_{\boldsymbol{K}},$$

$$\left(\frac{Z_O}{Z_C}\right)_{\boldsymbol{K}(\pm)} = \langle \boldsymbol{D}\rangle_{\boldsymbol{J}}.$$

Recognizing that ${}^{J}\Delta = {}^{V}\Delta$ and ${}^{K}\Delta = {}^{\mu}\Delta$, and applying lever operators to Eq. 15 in the main text, we obtain two of the desired linkage equations (Fig. S1, A and B):

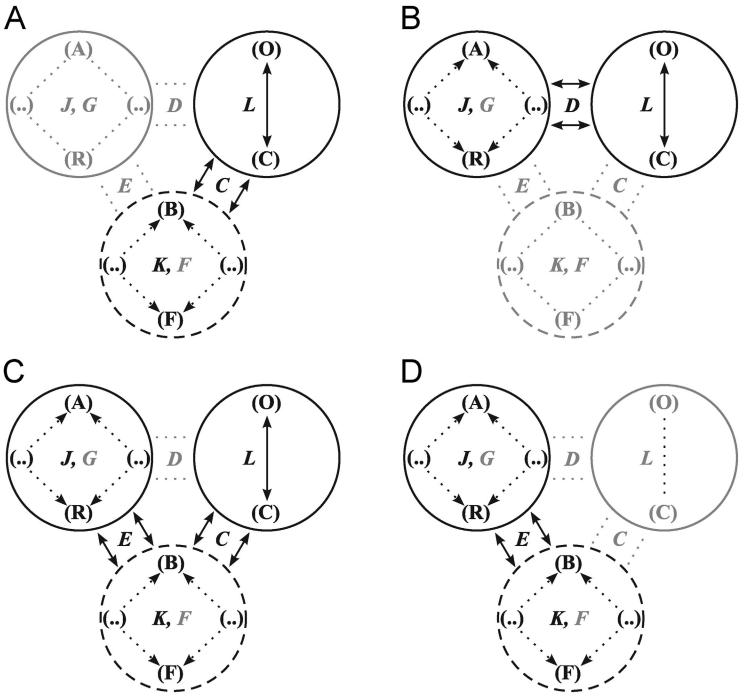

Figure S1. Sub-schemes used in the derivation of Eqs. 37a–d in the main text. Elements not participating in the linkage cycle are grayed out. (A) Conductance Hill analysis with μ as secondary activator (${}^{\mu}\Delta W_{H[g]\,V(\pm)}$). (B) Conductance Hill analysis with V as secondary activator (${}^{V}\Delta(W_{H[g]} + \mu_L)_{\mu(\pm)}$). (C) Electrical capacitance analysis with μ as secondary activator (${}^{\mu}\Delta W_{C[q]} = \Delta q_T\,{}^{\mu}\Delta V_M$). (D) "Limited" electrical capacitance analysis with μ as secondary activator and pore locked in closed or open position (${}^{\mu}\Delta W_{C[q]\,L(\pm)} = \Delta q_{\parallel}\,{}^{\mu}\Delta V_{M[C\text{ or }O]}$).

$$^{\mu}\Delta W_{H[g]V(\pm)} = -4\Delta W_{\boldsymbol{C}},$$

$$^{V}\Delta(W_{H[g]} + \eta_L)_{\mu(\pm)} = -4\Delta W_{\boldsymbol{D}}.$$

Note that in deriving these linkage relations from the above expressions for Z_O/Z_C, we invoked the last two rules in Table 3 of the main text, which specify that under limiting conditions, the CPF of a composite subsystem is equal to either 1.0 (negative endpoint) or the product of composite equilibrium constants and internal coupling factors (positive endpoint).

Choosing to perform the second round of parsing with respect to the composite voltage-sensor **J**, we expand Z_C and Z_O but write down only the first and last terms, corresponding to the limiting states $\boldsymbol{J}_{(-)}$ and $\boldsymbol{J}_{(+)}$:

$$Z_C = Z_{CR} + \ldots + \boldsymbol{JG}Z_{CA}, \tag{S4a}$$

$$Z_O = Z_{OR} + \ldots + \boldsymbol{JDG}Z_{OA}. \tag{S4b}$$

The second-order CPFs Z_{CR}, Z_{CA}, Z_{OR}, and Z_{OA} are all functions of the same polynomial f_2. In particular, we have $Z_{CR} = f_2(\boldsymbol{K}, \boldsymbol{F}, \boldsymbol{\chi})$, $Z_{OR} = f_2(\boldsymbol{KC}, \boldsymbol{F}, \boldsymbol{\chi}_L)$, $Z_{CA} = f_2(\boldsymbol{KE}, \boldsymbol{F}, \boldsymbol{\chi}_J)$, and $Z_{OA} = f_2(\boldsymbol{KCE}, \boldsymbol{F}, \boldsymbol{\chi}_{LJ})$. The CPF ratios that are of greatest interest to us (that is, related to the global work function $W_{C[q]}$) are the following:

$$\frac{Z_{OA}}{Z_{CR}} = \langle \boldsymbol{CE} \rangle_{\boldsymbol{K}},$$

$$\left\{ \frac{Z_{CA}}{Z_{CR}} \approx \frac{Z_{OA}}{Z_{OR}} \right\} = \langle \boldsymbol{E} \rangle_{\boldsymbol{K}}.$$

The approximation symbol in curly brackets is meant to show that, although the two CPF ratios are not exactly equal, they are similar in form and are equal for saturating concentrations. Applying the lever operator $^{\mu}\Delta$ to Eq. 33 in the main text (assuming Δn_L and Δn_J are zero), and substituting the above expression for Z_{OA}/Z_{CR}, we obtain the third linkage relation (Fig. S1 C):

$$^{\mu}\Delta W_{C[q]} = -4(\Delta W_{\boldsymbol{C}} + \Delta W_{\boldsymbol{E}}).$$

Recognizing that, with the pore locked in either the closed ($L_{(-)}$ = C) or open ($L_{(+)}$ = O) positions, the "limited" global work function $W_{C[q]L(\pm)}$ represents the selective activation of composite voltage sensor, and applying the lever operation $^{\mu}\Delta$ to the CPF ratios in curly brackets, we derive the last of the linkage equations (Fig. S1 D):

$$^{\mu}\Delta W_{C[q]L(\pm)} = -4\Delta W_{\boldsymbol{E}}.$$

Linkage relations used to discriminate between mechanisms of phenotype reversal in chimeric temperature-sensing TRP channels

One of several compelling pieces of evidence that a subset of TRP channels possesses a modular sensor for temperature regulation came from a chimera study by Brauchi et al. (2006), in which C-terminal domains between cold-activated TRPM8 and heat-activated TRPV1 channels were swapped, resulting in an exchange of temperature-sensing phenotypes, albeit with some loss in temperature sensitivity. It would appear from these experiments that the C terminus is a modular temperature sensor in the same way that the gating ring is a Ca^{2+} sensor for BK. For purposes of discussion, we will accept this at face value and illustrate the use of linkage analysis to distinguish between possible mechanisms of action, explaining the observed interchangeability of temperature phenotypes.

We begin by comparing ionic currents of the native TRPM8 channel (Brauchi et al., 2004) with those of the so-called CTctVR chimera, in which the C terminus of TRPV1 is spliced onto the core body of TRPM8 (Brauchi et al., 2006). At a fixed voltage of +60 mV, the native (cold-sensitive) TRPM8 channel is activated by an ~10°K decrease in temperature centered at 291°K. The heat-activated chimera CTctVR at +80 mV demonstrates a similarly steep response centered at 298°K (although somewhat attenuated and left-shifted compared with the native TRPV1 channel; see Yao et al., 2010). Assuming for the sake of argument that a single particle (K) is responsible for the observed temperature sensitivity, we may ascribe to it the following particle potential: $\eta_K = \Delta H_K - \Delta S_K T$, where ΔH and ΔS are the activation enthalpy and entropy per mole of substrate, respectively (assigned calorimetry units of cal/mol/K and kcal/mol). As demonstrated in the main text, the temperature sensitivities (10°K) of these channels correspond to entropy changes of $\Delta S_K = -251$ cal/mol/K for TRPM8 and $\Delta S_K = +251$ cal/mol/K for CTctVR.

In light of the tetrameric structure of TRP channels, we can model their temperature sensitivity using Scheme 1 (ignoring for the purpose of this discussion their small voltage sensitivity), in which the K particles are temperature activated as above, but the particle potential of the pore is constant: $\eta_L = \Delta H_L$. The entropy requirements can be split among the four K particles, with each requiring a minimum of 251 ÷ 4 = 63 cal/mol/K to denature. However, we'll arbitrarily allocate to each particle 100 cal/mol/K to allow for less than perfect efficiency in allosteric coupling with the pore. Hill analysis can be used to evaluate the interaction energy ΔW_C (in calorimetry units of RT) between K and L particles by applying the temperature lever operator $^{T}\Delta$ to $W_{H[g]}$.

We note that, although the value of $C = \exp(-\Delta W_C/RT)$ varies over the temperature range of interest, the term $1/RT$ responsible for temperature sensitivity (assuming ΔW_C is purely enthalpic) is canceled by the leading factor of RT in Eq. 15 of the main text (after substituting kT with RT), thereby predicting an exact difference of $-4\Delta W_C$ between the two T asymptotes in the linkage plot. Introducing an entropic component to the coupling energy ΔW_C generates a change in the slope of the positive asymptote by an amount ΔS_C, similar to a case where a small charge in the coupling factor G of Scheme 4 produced diverging asymptotes (Fig. 13 of main text).

It is worth emphasizing that the remarkable aspect of the chimera experiment is that the TRPM8 and TRPV1 C termini, which share a rough proximal homology despite being different in their distant sequences, conferred exactly opposite phenotypes when spliced onto the main body of TRPM8. Here it is important to remind ourselves that peptide denaturation is generally associated with an increase in entropy and is therefore favored by higher temperatures. If we assume that the folded form of the C terminus favors closing by holding together the S6 bundle helices of the internal gate (denaturation would presumably relax this arrangement, allowing the channel to open), then this would be con-

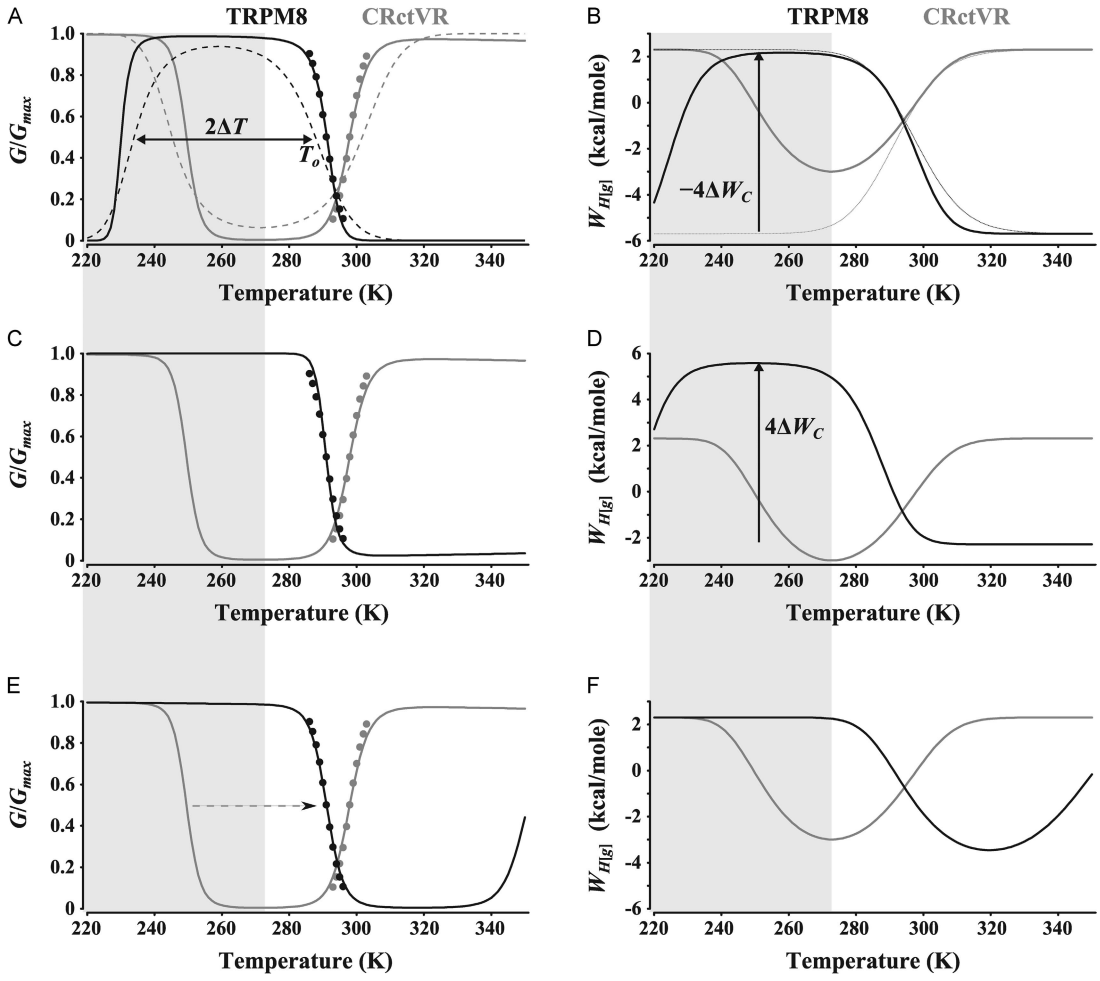

Figure S2. Scheme 1 models of temperature-sensitive TRP channels. All three schemes incorporate the following expression for the K particle potential: $\eta_K = (\Delta C_p - \Delta S_{Ko})(T - T_o) - \Delta C_p T \ln(T/T_o)$. (A) G-T curves for the cold-sensitive TRPM8 channel (black solid line) and the heat-sensitive chimera CRctCV (gray solid line). Parameter values are given by $T_c = 287.8°$K, $T_h = 287.8°$K, $\Delta S_o = 10^2$ cal/mol/K, $\Delta C_p = 10^3$ cal/mol/K, $\Delta H_L = +5.7$ kcal/mol, and $\Delta W_C = -2.0$ kcal/mol. The values of T_c, T_h, and ΔH_L were obtained by fits to the temperature curves of TRPM8 and CRctCV channels (closed circles) derived from the experimental work of Brauchi et al. (2004, 2006), as explained in the main text. Activity curves for the isolated K particles, equal to $K/(1 + K)$, are shown as dashed lines. (B) Conductance energy Hill plots ($W_{H[g]}$ vs. T) for TRPM8 and CRctCV models. Dotted lines indicate what the Hill curves would look like if ΔCp = 0. (C and D) Same as in A and B, except for the following parameter changes: $T_c = 277.7°$K, $\Delta H_L = -5.7$ kcal/mol, and $\Delta W_C = +2.0$ kcal/mol. (E and F) Same as in A and B, except for the following parameter change: $T_c = 353.7°$K. The shaded portion of the plots indicates temperature range where bath is frozen.

sistent with a "hot-activated" channel such as CTctVR. How then, reversing the usual direction of enquiry, does swapping out the TRPV1 C terminus in exchange for the original TRPM8 fragment reestablish cold sensitivity in the reconstituted TRPM8 channel?

There are at least three possible mechanisms to explain this result, each of which assumes allosteric linkage in the form of Scheme 1. The first explanation (see Fig. S2 A) is that, somehow, the mechanism by which the TRPM8 C terminus activates the pore is reversed in TRPV1 C terminus; that is, if we assume that the denatured form of the chimeric channel opens the pore, then the folded form of the cold-activated TRPM8 channel must close the channel. Mathematically, this is equivalent to reversing the sign of η_K, i.e., specifying that the folded conformation is the active state of K. Given the proximal sequence homologies between the TRPM8 and TRPV1 C termini (Brauchi et al., 2006), this seems unlikely but not impossible. The second explanation (Fig. S2 C) is superficially related to the first in that, rather than the denatured form of TRPM8 interacting positively to open the pore, it inhibits pore gating instead. In Scheme 1, this is mathematically equivalent to reversing the signs of both ΔW_C and ΔH_L. Although these first two mechanisms appear related in that they both involve interactions with the pore, they generate quantitatively different linkage plots, distinguishable by the second mechanism predicting an increased maximum value of TRPM8 $W_{H[g]}$ compared with TRPV1 (see Fig. S2, B and D).

A third possibility, recently put forward by Clapham and Miller (2011), can also be used to explain the chimera experiments. This relates to the hydrophobic effect, which is the primary source of entropy production during denaturation, and which generates a substantial increase in a denatured protein's heat capacity (C_p) compared with the folded state. The assumption of constant ΔC_p (Baldwin, 1986) leads to the following modified particle potential: $\eta_K = (\Delta C_p - \Delta S_{Ko})(T - T_o) - \Delta C_p T \ln(T/T_o)$ centered around the characteristic "melting" temperature $T_o = \Delta H_{Ko}/\Delta S_{Ko}$, as described in the main text. The value of T_o varies with channel type; thus, T_o can be renamed T_c for "cold-activated" TRPM8 and T_h for "hot-activated" TRPV1. The particle potential deviates from linearity if $\Delta C_p > 0$, reaching a maximal value at a lower temperature T_s when the transition entropy $\Delta S_K = \Delta S_{Ko} + \Delta C_p \ln(T/T_o)$ equals zero. The difference between the zero-energy or "melting" temperature T_o and the zero-entropy temperature T_s is given by $\Delta T = T_o(1 - \exp(-\Delta S_{Ko}/\Delta C_p))$, which, assuming $\Delta C_p >> \Delta S_{Ko}$, is roughly equal to $\Delta H_{Ko}/\Delta C_p$. This nonlinear temperature dependence of protein denaturation was included in all three proposed mechanisms for the purpose of Fig. S2, but it achieves special significance in the case of the third scenario, which postulates a second "melting" point occurring where the bell-shaped η_K versus T curve crosses zero at a lower temperature. In contrast to the "high temperature" crossing at T_o, the "low temperature" crossing occurring at $T \approx T_o - 2\Delta T$ has a positive slope, thereby conferring "cold activation" to the K particle. In principle, a normally "hot-activated" K particle can be turned into a "cold-activated" K particle simply by right-shifting the G-V on the temperature axis by an amount $2\Delta T$. This property of K could subsequently be transmitted to the pore gate through allosteric coupling (Fig. S2 E). A relatively small increase in ΔH_{Ko} (5.2 kcal/mol/K, or a 17% increase per subunit) is sufficient to transform the heat-activating TRPV1 C terminus into a cold-activating TRPM8 C terminus. The high temperature behavior of the TRPM8 Hill plot (characterized by an upward deflection in $W_{H[g]}$ preceding the conductance rise; see Fig. S2 F) is sufficiently different from that predicted by the first two mechanisms in that it could be used to support the third mechanism, if observed.

Calorimetry experiments could be used to quantify the thermal response of the excised C terminus by determining the values of ΔS_o, ΔH_o, and ΔC_p (Schellman, 1987). It is interesting to note that circular dichroism measurements of the TRPM8 C-terminal subunit demonstrates a T_o that is fairly right-shifted (~333°K; Tsuruda et al., 2006), indicating that, if the C terminus is the T-sensor, it must be strongly linked to pore activation to account for the observed temperature midpoint (~291°K) of the intact channel.

If Clapham and Miller's hypothesis is correct, the nonlinearity caused by hydrophobic effects in the activation potential of K would generate a roughly parabolic U-shaped plot of $W_{H[K]}$ versus T, unlike the straight line predicted for individual voltage and Ca^{2+} sensory particles of the BK channel. However, if K is not obligatorily linked to pore activation, but rather allosterically linked (Latorre et al., 2007; Matta and Ahern, 2007), a weakly temperature-dependent pore should flatten the $W_{H[g]}$ versus T curve at limiting temperatures (Fig. S2, B, D, and F). Distinguishing between the different linkage patterns seen in Fig. S2 using a limited range in temperature may be difficult from an experimental standpoint, but observing a characteristic pattern of linkage could lend support for a particular mechanism. Combining linkage methods with mutational analysis (see Chowdhury and Chanda, 2010) can also theoretically be used to distinguish between perturbations affecting the particle potential (intrinsic activation energy) of a putative T-sensor and allosteric factors coupling the sensor to the pore.

REFERENCES

Baldwin, R.L. 1986. Temperature dependence of the hydrophobic interaction in protein folding. *Proc. Natl. Acad. Sci. USA.* 83:8069–8072. http://dx.doi.org/10.1073/pnas.83.21.8069

Brauchi, S., P. Orio, and R. Latorre. 2004. Clues to understanding cold sensation: thermodynamics and electrophysiological analysis of the cold receptor TRPM8. *Proc. Natl. Acad. Sci. USA.* 101:15494–15499. http://dx.doi.org/10.1073/pnas.0406773101

Brauchi, S., G. Orta, M. Salazar, E. Rosenmann, and R. Latorre. 2006. A hot-sensing cold receptor: C-terminal domain determines thermosensation in transient receptor potential channels. *J. Neurosci.* 26:4835–4840. http://dx.doi.org/10.1523/JNEUROSCI.5080-05.2006

Chowdhury, S., and B. Chanda. 2010. Deconstructing thermodynamic parameters of a coupled system from site-specific observables. *Proc. Natl. Acad. Sci. USA.* 107:18856–18861. http://dx.doi.org/10.1073/pnas.1003609107

Clapham, D.E., and C. Miller. 2011. A thermodynamic framework for understanding temperature sensing by transient receptor potential (TRP) channels. *Proc. Natl. Acad. Sci. USA.* 108:19492–19497. http://dx.doi.org/10.1073/pnas.1117485108

Latorre, R., S. Brauchi, G. Orta, C. Zaelzer, and G. Vargas. 2007. ThermoTRP channels as modular proteins with allosteric gating. *Cell Calcium.* 42:427–438. http://dx.doi.org/10.1016/j.ceca.2007.04.004

Matta, J.A., and G.P. Ahern. 2007. Voltage is a partial activator of rat thermosensitive TRP channels. *J. Physiol.* 585:469–482. http://dx.doi.org/10.1113/jphysiol.2007.144287

Schellman, J.A. 1987. The thermodynamic stability of proteins. *Annu. Rev. Biophys. Biophys. Chem.* 16:115–137. http://dx.doi.org/10.1146/annurev.bb.16.060187.000555

Tsuruda, P.R., D. Julius, and D.L. Minor Jr. 2006. Coiled coils direct assembly of a cold-activated TRP channel. *Neuron.* 51:201–212. http://dx.doi.org/10.1016/j.neuron.2006.06.023

Yao, J., B. Liu, and F. Qin. 2010. Kinetic and energetic analysis of thermally activated TRPV1 channels. *Biophys. J.* 99:1743–1753. http://dx.doi.org/10.1016/j.bpj.2010.07.022